Lan et al. Nanoscale Research Letters (2020) 15:180
https://doi.org/10.1186/s11671-020-03409-7

Nanoscale Research Letters

Strain and Electric Field Controllable Schottky Barriers and Contact Types in Graphene-$MoTe_2$ van der Waals Heterostructure

Yu Lan[1*], Li-Xin Xia[2], Tao Huang[3], Weiping Xu[4], Gui-Fang Huang[3], Wangyu Hu[5] and Wei-Qing Huang[3*]

Abstract

Two-dimensional (2D) transition metal dichalcogenides with intrinsically passivated surfaces are promising candidates for ultrathin optoelectronic devices that their performance is strongly affected by the contact with the metallic electrodes. Herein, first-principle calculations are used to construct and investigate the electronic and interfacial properties of 2D $MoTe_2$ in contact with a graphene electrode by taking full advantage of them. The obtained results reveal that the electronic properties of graphene and $MoTe_2$ layers are well preserved in heterostructures due to the weak van der Waals interlayer interaction, and the Fermi level moves toward the conduction band minimum of $MoTe_2$ layer thus forming an *n* type Schottky contact at the interface. More interestingly, the Schottky barrier height and contact types in the graphene-$MoTe_2$ heterostructure can be effectively tuned by biaxial strain and external electric field, which can transform the heterostructure from an *n* type Schottky contact to a *p* type one or to Ohmic contact. This work provides a deeper insight look for tuning the contact types and effective strategies to design high performance $MoTe_2$-based Schottky electronic nanodevices.

Keywords: Schottky barrier, Graphene-$MoTe_2$ heterostructure, External electric field, Strain, First-principles calculations

Introduction

Two-dimensional (2D) layered crystals have attracted increasing interest due to their novel physical properties and potential applications in various fields since the discovery of graphene [1]. Unconventional features and performance, such as half-integer quantum Hall effect [2], Klein tunneling [3], and superconductivity [4], have been discovered in various 2D materials. For graphene, however, the Dirac cone type band structure without a band gap near the Fermi level hinders its direct applications in transistors. This has stimulated the searching for alternative materials from other 2D materials [5–14] with versatile properties, among which layered transition metal dichalcogenides (TMDs) have gained extensive attention. The band gaps of TMDs can be tuned from about 0.8 eV to 2.0 eV and are comparable with that of conventional semiconductors, enabling TMDs especially good candidates for optoelectronic applications. Being similar to graphite, most of TMDs are layered-structure materials with van der Waals (vdW) interaction between layers, thus can be exfoliated to few layers or a single layer [15, 16]. It is found that TMDs have thickness-dependent characteristics and would undergo an indirect-direct band gap transition [16, 17] when they are changed from bulk to few layers or monolayer. Monolayer TMDs have several structures, such as H phases and T phases (or T′ phases), while the H phases usually exhibit semiconducting characteristics.

As a member of TMDs, bulk $MoTe_2$ includes three interesting phases: hexagonal (2H, semiconducting) phase

* Correspondence: ylan@bnu.edu.cn; wqhuang@hnu.edu.cn
[1]College of Physics and Electronic Engineering, Hengyang Normal University, Hengyang 421002, China
[3]Department of Applied Physics, School of Physics and Electronics, Hunan University, Changsha 410082, China
Full list of author information is available at the end of the article

© The Author(s). 2020 **Open Access** This article is licensed under a Creative Commons Attribution 4.0 International License, which permits use, sharing, adaptation, distribution and reproduction in any medium or format, as long as you give appropriate credit to the original author(s) and the source, provide a link to the Creative Commons licence, and indicate if changes were made. The images or other third party material in this article are included in the article's Creative Commons licence, unless indicated otherwise in a credit line to the material. If material is not included in the article's Creative Commons licence and your intended use is not permitted by statutory regulation or exceeds the permitted use, you will need to obtain permission directly from the copyright holder. To view a copy of this licence, visit http://creativecommons.org/licenses/by/4.0/.

[18], monoclinic (1 T′, metallic) phase [19], and octahedral (T_d, type II Weyl semimetal) phase [20, 21], in which 2H-phase is the most stable one. 2H-phase $MoTe_2$ has an indirect band gap of about 1.0 eV for bulk and a direct band gap of about 1.1 eV for monolayer [22, 23], which indicates that the band gap is almost independent of the number of layers and it can be applied for the near-infrared photodetectors. For convenience, in the following text, 2H-$MoTe_2$ is simply referred as $MoTe_2$. Compared with other TMDs, $MoTe_2$ has many advantages, for example, the conductivity is lower [24], Seebeck coefficient is higher [24], and the sensing abilities are better [18, 25]. Combining the advantages of $MoTe_2$ and graphene, fabricating a type of heterostructure by graphene and $MoTe_2$ for device applications could be considered. Actually, recently vertical heterostructures based on 2D-layered-structure materials have been attracted increasing interests [26–33] due to the absence of dangling bonds at the surfaces of isolated components and weak Femi level pinning. For graphene-TMDs-based vertical heterostructures, experiments have confirmed their excellent high on-off ratio, high photo-response, low dark current, and good quantum efficiency [34–38], as compared with simple TMDs-based types. Though most of the reported graphene-TMDs-based vertical heterostructures are constructed with other TMDs, such as MoS_2, some experiments have investigated the graphene-$MoTe_2$ heterostructure [39–43] due to the unique electronic and optical properties of $MoTe_2$. It was reported [39] that the on-off ratio of the graphene-$MoTe_2$ vertical heterostructure is as high as ~$(0.5 - 1) \times 10^{-5}$, and the photo responsivity can reach 20 mAW^{-1}, which are comparable to the corresponding values of graphene-MoS_2 device. Later, based on graphene-$MoTe_2$-graphene vertical vdW heterostructure, a near-infrared photodetector was fabricated [40, 42] with a superior performance, including high photoresponsivity, high external quantum efficiency, rapid response and recovery processes, and free from an external source–drain power supply compared to other layered semiconductor photodetectors. Then, a graphene-$MoTe_2$ vdW vertical transistor which exhibits suitable V-shaped ambipolar characteristics [41] was reported. Hence, the graphene-$MoTe_2$ heterostructures are promising candidates for optoelectronic nanodevices with high responsivity, high-speed, and flexible. In this sense, it is essential to carry out a theoretical investigation on graphene-$MoTe_2$ vertical heterostructure which has not been reported yet.

For the metal-semiconductor heterostructure, the contact type (Schottky contact or Ohmic contact) has to be considered, because it determines the existence of rectifying characteristics or not for the heterostructure. For the Schottky contact, the Schottky barrier height (SBH) would play a key role on the behaviors of the corresponding devices [44] and has been investigated intensely. In order to achieve high performance for actual device applications, it would be desirable that SBH can be tuned. Many strategies have been proposed to modulate the SBH, among which applying an external electric field and biaxial strain are the most common ways.

In this paper, based on first-principles calculations, electronic structure, and external electronic field and strain dependence of the SBH of graphene-$MoTe_2$ heterostructure have been investigated. The calculated results demonstrate that the electronic properties of graphene and $MoTe_2$ monolayer are preserved quite well after being vertically stacked up as a heterostructure. The Schottky barrier of the heterostructure can be changed between *p* type and *n* type by applying an external electric field or strain, and the heterostructure can even reach the Ohmic contact when the external electric field or strain is strong enough.

Computational Methods

First-principle calculations have been carried out using the Vienna Ab-initio Simulation Package (VASP) [45–47] based on density functional theory (DFT). The projector augmented wave (PAW) [48] pseudopotentials were applied to model ion-electron interaction and the Perdew-Burke-Ernzerhof (PBE) generalized gradient approximation (GGA) [49] was used to treat electron exchange correlation. For all calculation, the DFT-D2 [50] method of Grimme representing the vdW interaction term are employed and the plane-wave cutoff energy is set to 600 eV. The convergence threshold is set to 10^{-6} eV for energy and 0.01 eV/Å for force. The Brillouin zone *k*-point mesh is set as $9 \times 9 \times 1$ within the Monkhost-Pack scheme. A vacuum space of 25 Å along the *z* direction is adopted to avoid the interaction between the neighboring layers. As it was revealed that the spin-orbit coupling effect on band structures of 2H-$MoTe_2$ is very weak [51], all of the calculations do not consider the spin-orbit coupling.

The graphene-$MoTe_2$ heterostructure is constructed by graphene and $MoTe_2$ monolayer via stacking the two 2D materials along the vertical direction. Both graphene and $MoTe_2$ adopt the hexagonal lattice and their lattice parameters are 2.46 Å [52] and 3.52 Å [53], respectively. Hence, the lattice mismatch is lower than the previous criterion of 5%. According to the structures of graphene and $MoTe_2$ monolayer, here, three typical stacking modes are considered: HS-1, HS-2, and HS-3, which are shown in Fig. 1. For HS-1 stacking mode, one Te atom just locates under the hollow site of the graphene lattice; for HS-2, one Te atom sits under one C atom site of the graphene lattice; for HS-3, one Te atom sits under another nonequivalent C atom site of the graphene lattice.

When the strain dependence of the SBH is investigated, strain is applied equally along the zigzag and armchair directions of graphene, respectively.

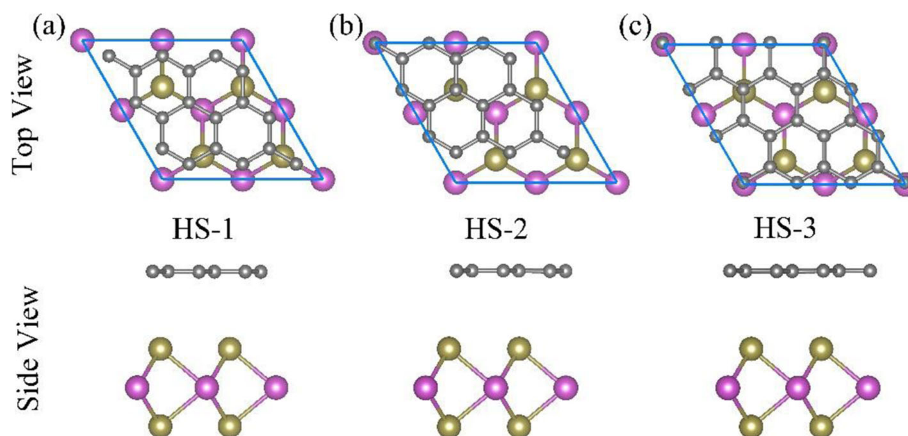

Fig. 1 Top view and side view of three typical stacking modes for the graphene-$MoTe_2$ heterostructure: (**a**) HS-1, (**b**) HS-2, (**c**) HS-3. The gray, pink, and green balls represent the carbon, molybdenum, and tellurium atoms, respectively

Results and Discussion

The lattice crystal structures for $MoTe_2$ monolayer and three typical stacking modes (HS-1, HS-2, and HS-3) of the graphene-$MoTe_2$ heterostructure have all been fully optimized. The obtained binding energies of the three typical stacking modes are all nearly the same, i.e., −0.85 eV, while the equilibrium interlayer distances of the three modes are all approximately equal to 3.53 Å. Hence, we solely focus on the HS-1 graphene-$MoTe_2$ heterostructure for the following discussion and omit “HS-1” for simplicity in the following text. The optimized geometry structures of $MoTe_2$ monolayer and graphene-$MoTe_2$ heterostructure are shown in Fig. 2. Obviously, $MoTe_2$ monolayer adopts the hexagonal lattice and the optimized lattice constant is 3.52 Å, which is consistent with the experiment results [53, 54]. It can be seen clearly from the band structure of $MoTe_2$ monolayer, as it is shown in Fig. 3, that $MoTe_2$ monolayer is a semiconductor with a band gap of 1.14 eV, which is also consistent with the experiment results [22, 23]. When graphene and $MoTe_2$ monolayer are vertically stacked up as a heterostructure, the equilibrium interlayer distance is 3.53 Å, which is comparable to the value of the Sb-$MoTe_2$ heterostructure (about 3.94 Å) [55]. It could also be seen from Fig. 2 that the geometry structures of the $MoTe_2$ layer and graphene layer in the graphene-$MoTe_2$ heterostructure almost remain the same as the original structures of $MoTe_2$ monolayer and graphene, which indicates the interaction between these two layers is weak. The binding energy of equilibrium structures −0.85 eV is lower than that of the Sb-$MoTe_2$ heterostructure (about −0.37 eV) [55], so the heterostructure is energetically stable. Both the equilibrium distance between two layers and binding energy are comparable to those of typical vdW graphene-based heterostructures, such as graphene-hydrogenated phosphorus carbide [56], graphene-AsSb [29], graphene-SMoSe and graphene-SeMoS [30], and graphene-phosphorene [57], indicating that the interaction between $MoTe_2$ and graphene is weak vdW type.

Actually, the charge redistribution and transfer would inevitably occur when graphene and $MoTe_2$ monolayer are stacked up to form the heterostructure. The 3D charge density difference in the graphene-$MoTe_2$ heterostructure defined as $\Delta\rho = \rho_H - \rho_G - \rho_{MT}$ has been calculated, where ρ_H, ρ_G, and ρ_{MT} are the charge densities of heterostructure, isolated graphene, and $MoTe_2$ monolayer, respectively. The result is shown in Fig. 4a, in which the blue and dark pink regions represent charge accumulation and depletion, respectively. Obviously, the blue region is just under the $MoTe_2$ layer, which indicates that the electrons accumulate around the $MoTe_2$ layer; while graphene layer is surrounded by the dark pink area, implying that the holes accumulate around the graphene layer. To see the property of the charge transfer more clearly, the planar average $\langle\Delta\rho\rangle$, which is defined as the average value of the 3D charge density difference $\Delta\rho$ in planes with z = const. that are parallel to the graphene layer, is shown as a blue line in Fig. 4a, where the negative and positive values represent electron depletion and accumulation, respectively. The result verifies that some electrons transfer from graphene layer to $MoTe_2$ layer, and there are oscillations in $\langle\Delta\rho\rangle$ in both the graphene and $MoTe_2$ layer. The electron localization function (ELF) is also plotted in Fig. 4b, from which it can be seen that the shape of ELF around the Te atom near the graphene layer is obviously different with that around the Te atom of the other side, suggesting the existence of interlayer vdW interaction in the heterostructure.

Many physical properties are determined by the band structures and density of states (DOS), and the calculated band structures and DOS of the graphene-$MoTe_2$ heterostructure are shown in Fig. 5, where the Fermi level is set to zero. The Dirac cone of the graphene layer

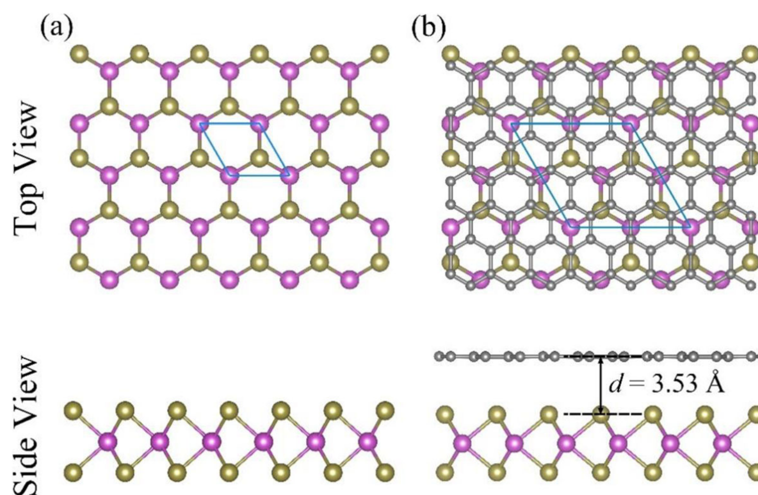

Fig. 2 Top view and side view of the optimized structures of (**a**) $MoTe_2$ monolayer and (**b**) graphene-$MoTe_2$ heterostructure. The gray, pink, and green balls represent the carbon, molybdenum, and tellurium atoms, respectively. The blue parallelograms denote the 2D unit cells

around the Fermi level is still well preserved; however, a band gap of about 10.6 meV is opened up. That is to say, there is a small but noticeable interlayer coupling in the heterostructure. The bands contributed by the $MoTe_2$ layer demonstrate that the semiconductor characteristics of $MoTe_2$ layer with a direct band gap are retained. The band gap of $MoTe_2$ layer is 0.85 eV in the heterostructure, which is changed compared with the result of 1.14 eV for the isolated $MoTe_2$ monolayer. One striking feature in Fig. 5 is that the band structure can be deemed as the simple sum of the bands of isolated layers. It is not surprising that interaction between the graphene layer and the $MoTe_2$ layer is insufficient to modify the characteristics of the band structure of each component in the heterostructure, so the interlayer interaction effect on the band structure is very weak. This further indicates that the vdW interaction dominates between $MoTe_2$ layer and graphene layer in the heterostructure, and thus preserving the intrinsic key properties.

The contact properties of heterostructures are of importance for device applications. A graphene-$MoTe_2$ heterojunction-based transistor has been designed, and

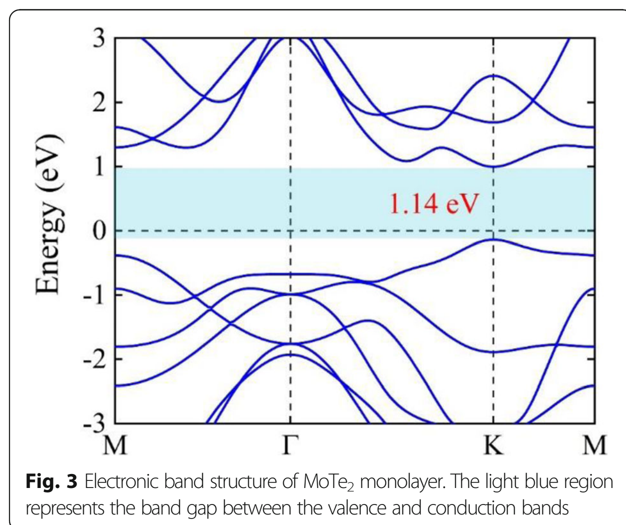

Fig. 3 Electronic band structure of $MoTe_2$ monolayer. The light blue region represents the band gap between the valence and conduction bands

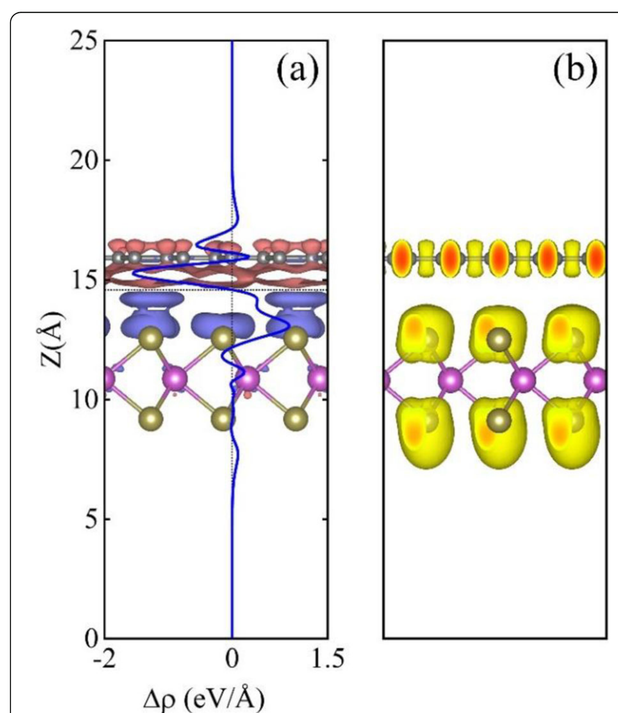

Fig. 4 **a** The 3D charge density difference and the average charge density difference (blue line) as a function of position in the graphene-$MoTe_2$ heterostructure along the *z* direction, where the blue and dark pink regions denote the accumulation and deficient of the electrons, respectively. The horizontal dashed line marks the central location between the graphene layer and $MoTe_2$ layer. **b** Electron localization function of the graphene-$MoTe_2$ heterostructure with the isovalue of 0.7

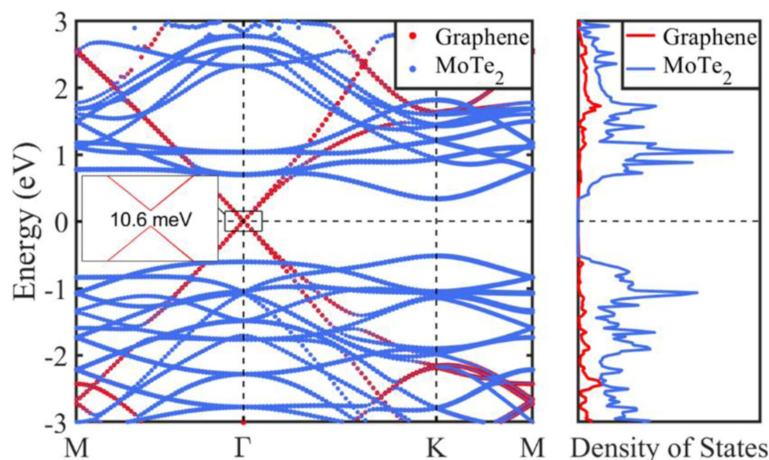

Fig. 5 Band structures and partial density of states of graphene layer and $MoTe_2$ layer in the graphene-$MoTe_2$ heterostructure

the schematic diagram is shown in Fig. 6a, where the $MoTe_2$ monolayer is used as the channel material and graphene as both source or drain and gate electrodes. Due to the difference in work functions of the metal and semiconductor, there is a band bending at the interface, which can be estimated by the Fermi level difference (ΔE_F), defined by $\Delta E_F = W_{G-MT} - W_{MT}$, where W_{G-MT} and W_{MT} are the work functions of the heterostructures and the corresponding $MoTe_2$ monolayer, respectively. The calculated W_{G-MT} and W_{MT} are 4.36 eV and 4.84 eV, respectively, as is shown in Fig. 6b. The results are consistent with the experimental values [39]. Consequently, the band bending (ΔE_F) is about 0.48 eV in the heterostructure, which is comparable to the result of graphene-hydrogenated phosphorus carbide heterostructure [56].

One of the most important contact properties of metal-semiconductor heterostructures is Schottky barrier at the vertical interface (between the graphene layer and the $MoTe_2$ layer), which determines the current flow across the interface of heterostructures thus playing a significant role in the corresponding device performance. In general, according to the types of the semiconductors in heterostructures, SBH is divided into n type and p type, respectively. The n type SBH (Φ_{Bn}) is defined as the energy difference between the conduction band minimum (CBM) of the semiconductor (E_C) and the Fermi level of the metal (E_F), i.e., $\Phi_{Bn} = E_C - E_F$. The p type SBH (Φ_{Bp}) is defined as the energy difference between the Fermi level of the metal and the valence band maximum (VBM) of the semiconductor (E_V), i.e., $\Phi_{Bp} = E_F - E_V$. The SBH results of the graphene-$MoTe_2$ heterostructure is shown in Fig. 6b. Due to the charge transfer, the Fermi level moves from the valence band side of the $MoTe_2$ monolayer to conduction band side of $MoTe_2$ layer in the heterostructure, which denotes that the SBH of the heterostructure is n type with the value of about 0.33 eV at the interface. That is to say, the charge conduction of the heterostructure will be mainly through electrons.

To improve the performance of heterostructure-based transistors, it would be desirable to tune the SBH. It is demonstrated that the SBH can be tuned via applying an external electric field and in-plane strain [29, 30, 58]. A series of calculations for the band structure of the heterostructure under different external electric fields have been made, and the results are shown in Fig. 7, where the direction for the positive external electric field points from the $MoTe_2$ layer to the graphene layer, while the negative value is along the opposite direction. In the Schottky contact region, Φ_{Bn} exhibits an approximately upward linear relationship with the electric field, while Φ_{Bp} behaves reversely. These results suggest that the positive and negative electric fields enable the Fermi level to shift toward the VBM and CBM of the $MoTe_2$ layer in the heterostructure, respectively. Under the negative electric field, Φ_{Bn} is smaller than Φ_{Bp} all the time, indicating that the Schottky barrier is n type. When the positive electric field is a little greater than zero, Φ_{Bn} begins to be greater than Φ_{Bp}, which means the Schottky barrier is changed from n type to p type at the graphene-$MoTe_2$ interface. It is obviously that the band gap (approximately equals to the sum of Φ_{Bn} and Φ_{Bp}) of the $MoTe_2$ layer almost remains constant under the external electric field, which denotes that the external field has little effect on the pristine electronic properties. This can be understood as follows: although the external electric field can change the energy eigenvalues of the valence electron such as CBM and VBM, their relative values are unchanged, resulting in the band gap remaining constant. In other words, the external electric field could not change the band structure except the band bending. It can be also seen clearly from Fig. 7 that the SBH becomes negative when the positive electric field is greater than 1.0 V/nm, which means that electrons from graphene would be injected into

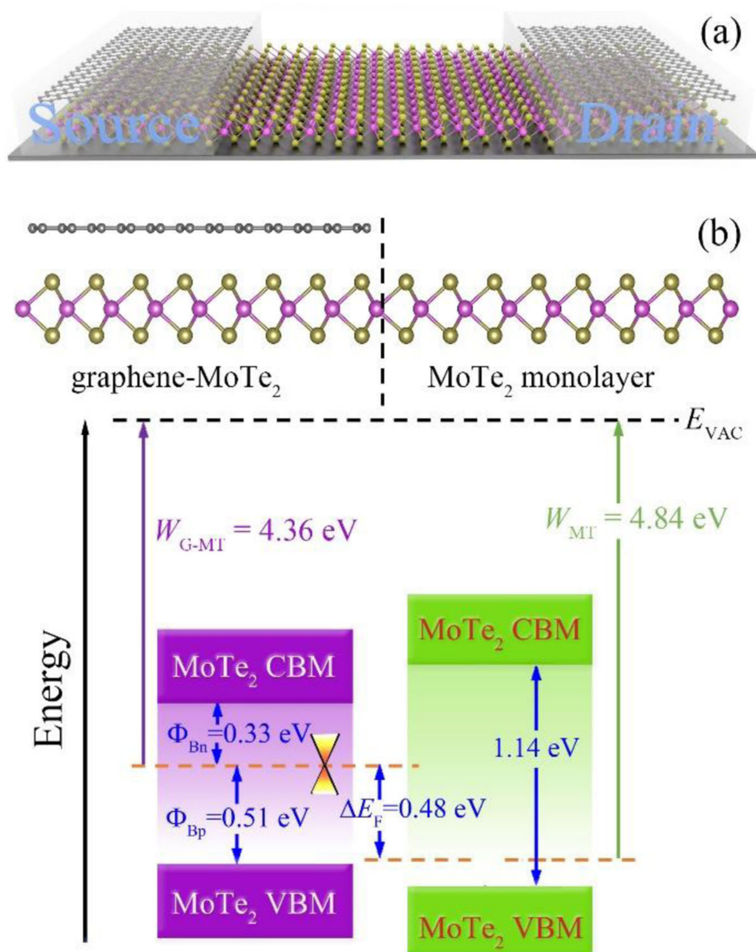

Fig. 6 a The schematic diagram of a graphene-$MoTe_2$ heterostructure based transistor. **b** Band alignment of graphene-$MoTe_2$ heterostructure with respect to vacuum level, where the red cone represents the position of the Dirac point of graphene layer in the heterostructure. CBM and VBM represent conduction band minimum and valence band maximum, respectively. $W_{G\text{-}MT}$ and W_{MT} are the work functions of graphene-$MoTe_2$ heterostructure and $MoTe_2$ monolayer, respectively

$MoTe_2$ without any barrier, indicating that $MoTe_2$ possesses a metallic conductivity, and thus realizing a Schottky-to-Ohmic contact transition. For the negative electric field when the intensity exceeds 1.0 V/nm, the heterostructure could also be tuned to the Ohmic contact. All these results demonstrate that applying an external electric field is an effective strategy to modulate the SBH and contact type for the graphene-$MoTe_2$ heterostructure.

The SBH as a function of the in-plane biaxial strain is also calculated and the results are displayed in Fig. 8. For applying the biaxial strain, the z coordinate of the Te atoms are relaxed while the positions of other atoms remain fixed after changing the size of the unit cell. It is shown that strain can also tune the SBH of the heterostructure between n type and p type and drive the heterostructure to approach the Ohmic contact. The behaviors of strain dependence of SBH are very different with that of the electric field dependence. The situation becomes much more complex. For a wide strain range, Φ_{Bn} is smaller than Φ_{Bp}, while only in a narrow tensile strain range Φ_{Bp} maintains smaller than Φ_{Bn}. That is to say, the strain range of n-type SBH (the strain is about −10 ~ 4%) is much wider than that of the p type (about 4 ~ 7%). When the tensile strain reaches 7% and the compressive strain reaches 10%, the Ohmic contact for the heterostructure also appears. It is worth noting that the band gap of the $MoTe_2$ layer in the heterostructure would change strongly with the variation of the strain in the Schottky contact region, which is strongly different with the results of the electric field case. When the lattices are under strain, they would deviate from the equilibrium state, thus causing the change of the band structure. In fact, not only the value of band gap but also the type of band gap (direct or indirect) would be change by strain. For small strain, $MoTe_2$ layer remains a direct band gap while it changes to indirect band gap for large strain. Here, it should be pointed out that for a real

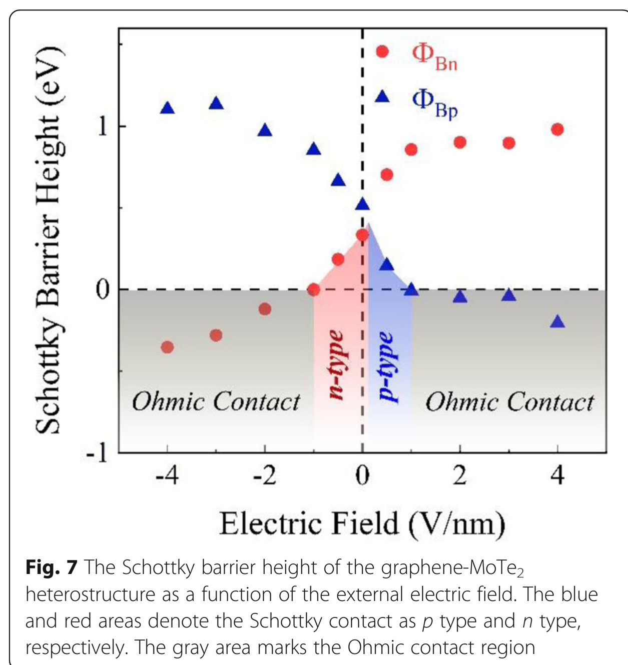

Fig. 7 The Schottky barrier height of the graphene-$MoTe_2$ heterostructure as a function of the external electric field. The blue and red areas denote the Schottky contact as *p* type and *n* type, respectively. The gray area marks the Ohmic contact region

transistor the actual conditions to realize the Schottky-to-Ohmic contact transition may be somewhat different with the calculated results due to the actual situations.

The above results suggest that both applying an external electric field and in-plane biaxial strain are effective methods to control SBH and the type of contact of the graphene-$MoTe_2$ heterostructure, which is indispensable to design 2D vdW heterostructure based field-effect transistors. Furthermore, the graphene-$MoTe_2$ heterostructure can be applied for tunable Schottky diodes in nanoelectronic and optoelectronic devices.

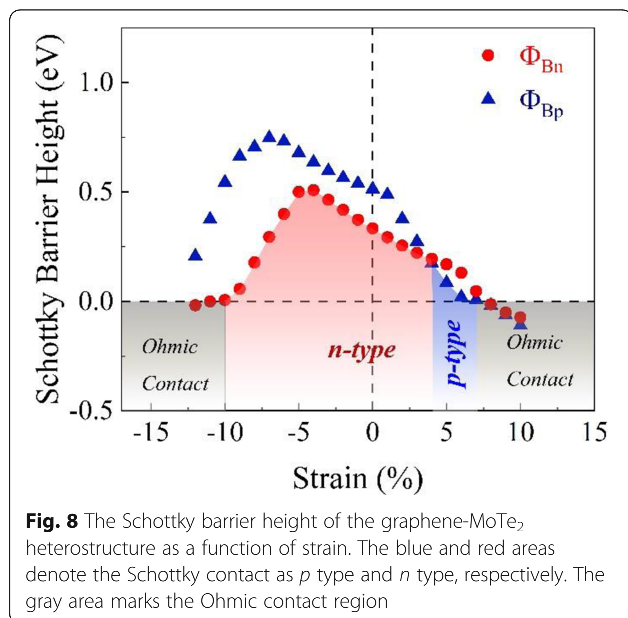

Fig. 8 The Schottky barrier height of the graphene-$MoTe_2$ heterostructure as a function of strain. The blue and red areas denote the Schottky contact as *p* type and *n* type, respectively. The gray area marks the Ohmic contact region

Conclusions

In summary, the band structures of the graphene-$MoTe_2$ heterostructure under different electric fields and biaxial strains have been systematically investigated based on first-principle calculations. The electronic structures of graphene and $MoTe_2$ are well preserved after being stacked up together along the vertical direction, which suggests that the interlayer interaction of the heterostructure belongs to the vdW type. However, the Fermi level moves toward CBM of the $MoTe_2$ layer after the formation of the heterostructure, i.e., the Schottky contacts are *n* type with a 0.33 eV SBH. The SBH and the type of contacts at the heterostructure interface can be effectively modulated by applying an external electric field or strain. When an electric field is applied, in the Schottky contact region, the *n* type SBH exhibits an approximately upward linear relationship with the electric field, and *p* type SBH behaves reversely. The heterostructure can be tuned to the Ohmic contact for an electric field which is greater than 1.0 V/nm at both positive and negative sides. For the case of applying biaxial strain, the situation is more complex than the electric field case. The strain range of *n* type SBH is much wider than that of the *p* type. When the tensile strain reaches 7% or the compressive strain reaches 10%, the Ohmic contact also appears. All the results demonstrate that applying an electric field or strain is a good way to control of the SBH as well as the type of contact of the heterostructure, even drive the system into the Ohmic contact. These features are quite significant for designing high performance nanoelectronic and optoelectronic devices.

Abbreviations

2D: Two-dimensional; TMDs: Transition metal dichalcogenides; vdW: Van der Waals; SBH: Schottky barrier height; DFT: Density functional theory; PAW: Projector augmented wave; PBE: Perdew-Burke-Ernzerhof; GGA: Generalized gradient approximation; DOS: Density of states; CBM: Conduction band minimum; VBM: Valence band maximum

Acknowledgements

The authors would like to thank Sen Zhang, Meng-Qi Cheng, Qing Chen, Kun Liang, and Yuwen Xiao for helpful discussions.

Authors' Contributions

YL and WQ proposed the work and revised the paper. YL conducted the calculations and wrote the manuscript. All authors have devoted valuable discussions. All authors read and approved the final manuscript.

Funding

The authors are not currently in receipt of any funding which relates to the research presented in this paper.

Availability of Data and Materials

The datasets supporting the conclusions of this article are included within the article, and further information about the data and materials could be made available to the interested party under a motivated request addressed to the corresponding author.

Competing Interests

The authors declare that they have no competing interests.

Author details
[1]College of Physics and Electronic Engineering, Hengyang Normal University, Hengyang 421002, China. [2]Department of Physics, Kashi University, Kashi 844006, China. [3]Department of Applied Physics, School of Physics and Electronics, Hunan University, Changsha 410082, China. [4]Dingcheng District Power Supply Branch of Changde Power Supply Company, State Grid, Changde 415100, China. [5]School of Materials Science and Engineering, Hunan University, Changsha 410082, China.

Received: 14 July 2020 Accepted: 14 September 2020
Published online: 21 September 2020

References

1. Novoselov KS, Geim AK, Morozov SV, Jiang D, Zhang Y, Dubonos SV, Grigorieva IV, Firsov AA (2004) Electric field effect in atomically thin carbon films. Science 306:666
2. Wu X, Hu Y, Ruan M, Madiomanana NK, Hankinson J, Sprinkle M, Berger C, WAd H (2009) Half integer quantum Hall effect in high mobility single layer epitaxial graphene. Appl Phys Lett 95:223108
3. Young AF, Kim P (2009) Quantum interference and Klein tunnelling in graphene heterojunctions. Nat Phys 5:222–226
4. Cao Y, Fatemi V, Fang S, Watanabe K, Taniguchi T, Kaxiras E, Jarillo-Herrero P (2018) Unconventional superconductivity in magic-angle graphene superlattices. Nature 556:43–50
5. Li Y-Y, Zhou B-X, Zhang H-W, Ma S-F, Huang W-Q, Peng W, Hu W, Huang G-F (2019) Doping-induced enhancement of crystallinity in polymeric carbon nitride nanosheets to improve their visible-light photocatalytic activity. Nanoscale 11:6876–6885
6. Li B, Si Y, Fang Q, Shi Y, Huang W-Q, Hu W, Pan A, Fan X, Huang G-F (2020) Hierarchical self-assembly of well-defined Louver-like P-doped carbon nitride nanowire arrays with highly efficient hydrogen evolution. Nano-Micro Lett 12:52
7. Zhang J, Jiang W-J, Niu S, Zhang H, Liu J, Li H, Huang G-F, Jiang L, Huang W-Q, Hu J-S, Hu W (2020) Organic small molecule activates transition metal foam for efficient oxygen evolution reaction. Adv Mater 32:1906015
8. Cheng M-Q, Chen Q, Yang K, Huang W-Q, Hu W-Y, Huang G-F (2019) Penta-graphene as a potential gas sensor for NO_x detection. Nanoscale Res Lett 14:306
9. Li X, Li Y, Zhang X, Long M, Zhou G (2019) Spin-resolved electronic and transport properties of graphyne-based nanojunctions with different N-substituting positions. Nanoscale Res Lett 14:299
10. Cao L, Li X, Zuo M, Jia C, Liao W, Long M, Zhou G (2019) Perfect negative differential resistance, spin-filter and spin-rectification transport behaviors in zigzag-edged δ-graphyne nanoribbon-based magnetic devices. J Magn Magn Mater 485:136–141
11. Dong Y, Zeng B, Zhang X, Li D, He J, Long M (2019) Study on the strain-induced mechanical property modulations in monolayer tellurene. J Appl Phys 125:064304
12. Liu J, Pantelides ST (2018) Electrowetting on 2D dielectrics: a quantum molecular dynamics investigation. J Phys Condens Matter 30:375001
13. Liu J, Pantelides ST (2018) Anisotropic thermal expansion of group-IV monochalcogenide monolayers. Appl Phys Express 11:101301
14. Liu J, Pantelides ST (2019) Pyroelectric response and temperature-induced α - β phase transitions in α -In 2 Se 3 and other α -III 2 VI 3 (III = Al, Ga, In; VI = S, Se) monolayers. 2D. Mater 6:025001
15. Novoselov KS, Jiang D, Schedin F, Booth TJ, Khotkevich VV, Morozov SV, Geim AK, Rice TM (2005) Two-dimensional atomic crystals. Proc Natl Acad Sci USA 102:10451–10453
16. Mak KF, Lee C, Hone J, Shan J, Heinz TF (2010) Atomically thin MoS_2: a new direct-gap semiconductor. Phys Rev Lett 105:136805
17. Splendiani A, Sun L, Zhang Y, Li T, Kim J, Chim C-Y, Galli G, Wang F (2010) Emerging photoluminescence in monolayer MoS_2. Nano Lett 10:1271–1275
18. Keum DH, Cho S, Kim JH, Choe D-H, Sung H-J, Kan M, Kang H, Hwang J-Y, Kim SW, Yang H, Chang KJ, Lee YH (2015) Bandgap opening in few-layered monoclinic $MoTe_2$. Nat Phys 11:482–486
19. Tan Y, Luo F, Zhu M, Xu X, Ye Y, Li B, Wang G, Luo W, Zheng X, Wu N, Yu Y, Qin S, Zhang X-A (2018) Controllable 2H-to-1 T' phase transition in few-layer $MoTe_2$. Nanoscale 10:19964–19971
20. Huang L, McCormick TM, Ochi M, Zhao Z, Suzuki M-T, Arita R, Wu Y, Mou D, Cao H, Yan J, Trivedi N, Kaminski A (2016) Spectroscopic evidence for a type II Weyl semimetallic state in $MoTe_2$. Nat Mater 15:1155–1160
21. Berger AN, Andrade E, Kerelsky A, Edelberg D, Li J, Wang Z, Zhang L, Kim J, Zaki N, Avila J, Chen C, Asensio MC, Cheong S-W, Bernevig BA, Pasupathy AN (2018) Temperature-driven topological transition in 1 T'-$MoTe_2$. npj Quantum Mater 3:2
22. Ruppert C, Aslan OB, Heinz TF (2014) Optical properties and band gap of single- and few-layer $MoTe_2$ crystals. Nano Lett 14:6231–6236
23. Lezama IG, Arora A, Ubaldini A, Barreteau C, Giannini E, Potemski M, Morpurgo AF (2015) Indirect-to-direct band gap crossover in few-layer $MoTe_2$. Nano Lett 15:2336–2342
24. Balendhran S, Walia S, Nili H, Ou JZ, Zhuiykov S, Kaner RB, Sriram S, Bhaskaran M, Kalantar-zadeh K (2013) Two-dimensional molybdenum trioxide and dichalcogenides. Adv Funct Mater 23:3952–3970
25. Feng Z, Xie Y, Chen J, Yu Y, Zheng S, Zhang R, Li Q, Chen X, Sun C, Zhang H, Pang W, Liu J, Zhang D (2017) Highly sensitive $MoTe_2$ chemical sensor with fast recovery rate through gate biasing. 2D Mater 4:025018
26. Hamm JM, Hess O (2013) Two two-dimensional materials are better than one. Science 340:1298–1299
27. Geim AK, Grigorieva IV (2013) Van der Waals heterostructures. Nature 499: 419–425
28. Liu Y, Stradins P, Wei S-H (2016) Van der Waals metal-semiconductor junction: weak Fermi level pinning enables effective tuning of Schottky barrier. Sci Adv 2:e1600069
29. Li H, Cui Y, Li D, Luo H (2018) Tuning the band alignment of p-type graphene-AsSb Schottky contact by electric field. J Appl Phys 124:204301
30. Li Y, Wang J, Zhou B, Wang F, Miao Y, Wei J, Zhang B, Zhang K (2018) Tunable interlayer coupling and Schottky barrier in graphene and Janus MoSSe heterostructures by applying an external field. Phys Chem Chem Phys 20:24109–24116
31. Tang K, Qi W, Li Y, Wang T (2018) Electronic properties of van der Waals heterostructure of black phosphorus and MoS_2. J Phys Chem C 122:7027–7032
32. Zhu J, Ning J, Wang D, Zhang J, Guo L, Hao Y (2019) High-performance two-dimensional InSe field-effect transistors with novel sandwiched ohmic contact for sub-10 nm nodes: a theoretical study. Nanoscale Res Lett 14:277
33. Gu H, Tian F, Zhang C, Xu K, Wang J, Chen Y, Deng X, Liu X (2019) Recovery performance of Ge-doped vertical GaN Schottky barrier diodes. Nanoscale Res Lett 14:40
34. Britnell L, Ribeiro RM, Eckmann A, Jalil R, Belle BD, Mishchenko A, Kim Y-J, Gorbachev RV, Georgiou T, Morozov SV, Grigorenko AN, Geim AK, Casiraghi C, Neto AHC, Novoselov KS (2013) Strong light-matter interactions in heterostructures of atomically thin films. Science 340:1311–1314
35. Roy K, Padmanabhan M, Goswami S, Sai TP, Ramalingam G, Raghavan S, Ghosh A (2013) Graphene–MoS_2 hybrid structures for multifunctional photoresponsive memory devices. Nat Nanotechnol 8:826–830
36. Zhang W, Chuu C-P, Huang J-K, Chen C-H, Tsai M-L, Chang Y-H, Liang C-T, Chen Y-Z, Chueh Y-L, He J-H, Chou M-Y, Li L-J (2014) Ultrahigh-gain photodetectors based on atomically thin graphene-MoS_2 heterostructures. Sci Rep 4:3826
37. Koppens FHL, Mueller T, Avouris P, Ferrari AC, Vitiello MS, Polini M (2014) Photodetectors based on graphene, other two-dimensional materials and hybrid systems. Nat Nanotechnol 9:780–793
38. Rathi S, Lee I, Lim D, Wang J, Ochiai Y, Aoki N, Watanabe K, Taniguchi T, Lee G-H, Yu Y-J, Kim P, Kim G-H (2015) Tunable electrical and optical characteristics in monolayer graphene and few-layer MoS_2 heterostructure devices. Nano Lett 15:5017–5024
39. Kuiri M, Chakraborty B, Paul A, Das S, Sood AK, Das A (2016) Enhancing photoresponsivity using $MoTe_2$-graphene vertical heterostructures. Appl Phys Lett 108:063506
40. Zhang K, Fang X, Wang Y, Wan Y, Song Q, Zhai W, Li Y, Ran G, Ye Y, Dai L (2017) Ultrasensitive near-infrared photodetectors based on a graphene-$MoTe_2$-graphene vertical van der Waals heterostructure. ACS Appl Mater Interfaces 9:5392–5398
41. Pan C, Fu Y, Wang J, Zeng J, Su G, Long M, Liu E, Wang C, Gao A, Wang M, Wang Y, Wang Z, Liang S-J, Huang R, Miao F (2018) Analog circuit applications based on ambipolar graphene/$MoTe_2$ vertical transistors. Adv Electron Mater 4:1700662
42. Hu R-X, Ma X-L, An C-H, Liu J (2019) Visible-to-near-infrared photodetector based on graphene–$MoTe_2$–graphere heterostructure. Chin Phys B 28:117802
43. Castelino R, Pham TT, Felten A, Sporken R (2020) Substrate temperature dependence of the crystalline quality for the synthesis of pure-phase $MoTe_2$ on graphene/6H-SiC(0001) by molecular beam epitaxy. Nanotechnology 31: 115702
44. Tung RT (2014) The physics and chemistry of the Schottky barrier height. Appl Phys Rev 1:011304

45. Kresse G, Furthmüller J (1996) Efficiency of ab-initio total energy calculations for metals and semiconductors using a plane-wave basis set. Comput Mater Sci 6:15–50
46. Grimme S, Antony J, Ehrlich S, Krieg H (2010) A consistent and accurate ab initio parametrization of density functional dispersion correction (DFT-D) for the 94 elements H-Pu. J Chem Phys 132:154104
47. Grimme S, Ehrlich S, Goerigk L (2011) Effect of the damping function in dispersion corrected density functional theory. J Comput Chem 32:1456–1465
48. Blöchl PE (1994) Projector augmented-wave method. Phys Rev B 50:17953–17979
49. Perdew JP, Burke K, Ernzerhof M (1996) Generalized gradient approximation made simple. Phys Rev Lett 77:3865–3868
50. Grimme S (2004) Accurate description of van der Waals complexes by density functional theory including empirical corrections. J Comput Chem 25:1463–1473
51. Bera A, Singh A, Muthu DVS, Waghmare UV, Sood AK (2017) Pressure-dependent semiconductor to semimetal and Lifshitz transitions in 2H-MoTe2: Raman and first-principles studies. J Phys Condens Matter 29:105403
52. Castro Neto AH, Guinea F, Peres NMR, Novoselov KS, Geim AK (2009) The electronic properties of graphene. Rev Mod Phys 81:109–162
53. Wilson JA, Yoffe AD (1969) The transition metal dichalcogenides discussion and interpretation of the observed optical, electrical and structural properties. Adv Phys 18:193–335
54. Sugai S, Ueda T (1982) High-pressure Raman spectroscopy in the layered materials 2H-MoS_2, 2H-$MoSe_2$, and 2H-$MoTe_2$. Phys Rev B 26:6554–6558
55. Bo M, Li H, Huang Z, Li L, Yao C (2020) Bond relaxation and electronic properties of two-dimensional Sb/$MoSe_2$ and Sb/$MoTe_2$ van der Waals heterostructures. AIP Adv 10:015321
56. Huang T, Chen Q, Cheng M-Q, Huang W-Q, Hu W, Huang G-F (2019) Tunable Schottky barrier in van der Waals heterostructures of graphene and hydrogenated phosphorus carbide monolayer: first-principles calculations. J Phys D Appl Phys 52:305104
57. Padilha JE, Fazzio A, da Silva AJR (2015) van der Waals heterostructure of phosphorene and graphene: tuning the schottky barrier and doping by electrostatic gating. Phys Rev Lett 114:066803
58. Yu ZG, Zhang Y-W, Yakobson BI (2016) Strain-robust and electric field tunable band alignments in van der Waals WSe_2–graphene heterojunctions. J Phys Chem C 120:22702–22709

Publisher's Note

Springer Nature remains neutral with regard to jurisdictional claims in published maps and institutional affiliations.

Submit your manuscript to a SpringerOpen journal and benefit from:

► Convenient online submission
► Rigorous peer review
► Open access: articles freely available online
► High visibility within the field
► Retaining the copyright to your article

Submit your next manuscript at ► springeropen.com